# Direct Measurement of Ice-Ablator Interface Motion for Instability Mitigation in Indirect Drive ICF Implosions

Alexandre Do,* Christopher R. Weber, Eduard L. Dewald, Daniel T. Casey, Daniel S. Clark, Shahab F. Khan, Otto L. Landen, Andrew G. MacPhee, and Vladimir A. Smalyuk
*Lawrence Livermore National Laboratory, Livermore, California 94551, USA*

(Received 26 July 2022; revised 12 October 2022; accepted 2 November 2022; published 15 November 2022)

In indirect drive inertial confinement fusion (ICF) implosions hydrodynamic instability growth at the imploding capsule ablator-DT fuel interface can reduce fuel compressibility and inject ablator into the hot spot hence reducing hot spot pressure and temperature. As a mitigation strategy, a gentle acceleration of this interface is predicted by simulations and theory to significantly reduce this instability growth in the early stage of the implosion. We have performed high-contrast, time-resolved x-ray refraction enhanced radiography (RER) to accurately measure the level of acceleration as a function of the initial laser drive time history for indirect-drive implosions on the National Ignition Facility. We demonstrate a transition from no acceleration to $20 \pm 1.8$ $\mu m\,ns^{-2}$ acceleration by tweaking the drive that should reduce the initial instabilities by an order of magnitude at high modes.

DOI: 10.1103/PhysRevLett.129.215003

Indirect drive inertial confinement fusion (ICF) [1–5] experiments are using the 192 laser beams of the National Ignition Facility (NIF) [2] with up to 2 MJ energy with the goal of imploding capsules to thermonuclear ignition. The laser energy is converted to thermal x rays inside a high $Z$ cavity (hohlraum). A $\sim 1$ mm radius capsule (ablator) is filled with an ice layer of deuterium-tritium (DT) fuel and is ablated by the x rays, causing the capsule to implode, compress and heat the DT, and ignite. A capsule inner layer doped with a mid-to-high $Z$ material shields the ice-ablator interface from hohlraum hard x-ray preheat, resulting in an increased fuel compression [6].

Recent implosions using high density carbon (HDC) diamond capsules have achieved record fusion yields of up to 170 kJ [7,8]. At the same time, the fusion neutron yields are still below what was expected from hydrodynamic simulations and the imploded fuels are less compressed than intended [9,10]. Increasing the compression of the DT ice fuel during stagnation is essential for increasing fuel burn up and hence achieving multi-MJ yields in ICF implosions. One hypothesis for reduced compression is the fuel-ablator mixing at their interface. This mixing can also lead to ablator material entering and radiatively cooling the hot spot [11]. Figure 1 shows the laser drive for a typical 3-shock implosion using high density carbon ablator, called here the HDC design [12,13]. The first shock reaches the fuel-ablator interface at $t = 3.2$ ns, driving a constant fuel-ablator interface velocity until the second shock arrives about 1 ns later, itself overtaken by the third shock such that all three shocks merge at the DT fuel-gas boundary. Any shock that leaves a fuel-ablator interface with constant velocity leads to an inherently linearly growing perturbation growth due to the Richtmyer-Meshkov instability (RM) [14–16]. Any shock phase perturbation can grow through the Rayleigh-Taylor (RT) [17,18] instability during the subsequent acceleration phase [19,20].

Initially the concept of adiabat shaping at the ablation front was proposed [21] and developed with direct drive implosions on the OMEGA laser [22–24] to mitigate the RT instabilities through higher ablation velocity. Similarly, it was proposed, as stabilization method of the RM phase, to use a "tailored density profile" [25] to reduce initial modulations [26–29] that would also stabilize the later RT

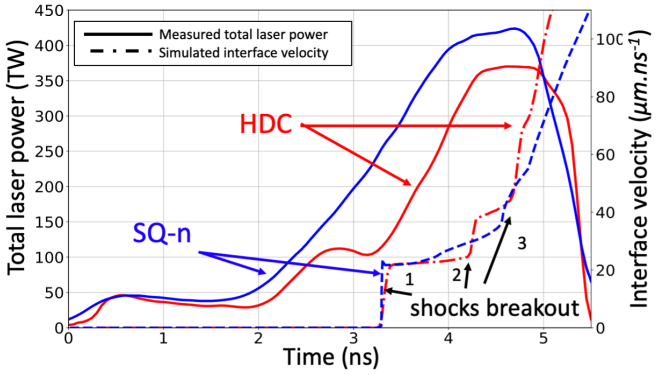


FIG. 1. Total laser drive for the HDC shot N210801 (plain red), SQ-n shot N211030 (plain blue), simulated fuel-ablator interface velocity for HDC shot (dotted-dashed red), and SQ-n shot (dashed blue). First, second, and third shock breakout are highlighted. The second one is only visible in the case of HDC. Note that the SQ-n data and simulations have been shifted 260 ps later to allow the comparison with the HDC results.

 

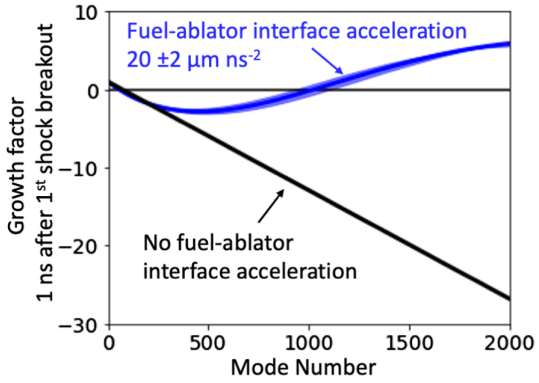


FIG. 2. Simulation of the growth factor of Richtmyer-Meshkov (RM) and Rayleigh-Taylor (RT) instabilities versus mode number 1 ns after the first shock breakout [31]. In the early phase of the implosion, or RM phase, if the fuel-ablator interface is not accelerating, the instabilities are growing linearly as shown by the black curve. Oppositely, in the presence of an acceleration, RT develops in addition to RM, resulting in instability oscillation rather than a linear growth as shown by the blue curve, thus increasing the stability.

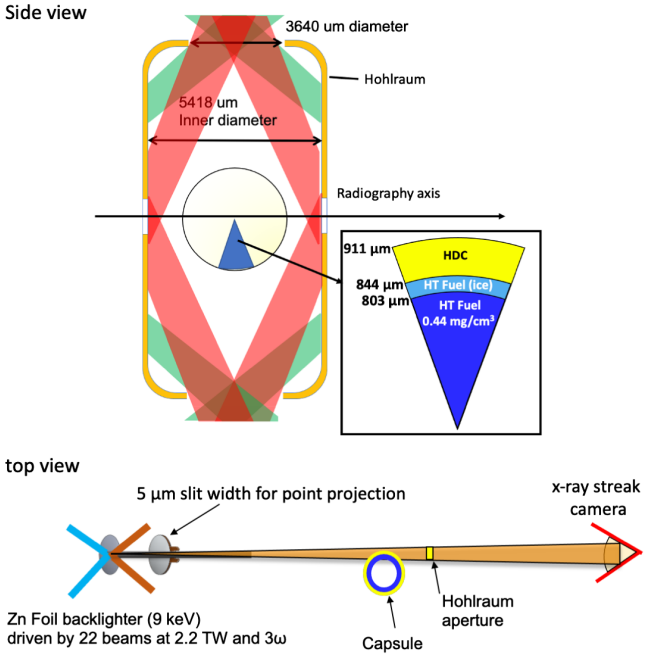


FIG. 3. Side (top) and top (bottom) view schematic of the experiment. A hohlraum is irradiated with 160 beams with inner (red) and outer beams (green). The RER image of an equatorial capsule limb at its midplane is taken through HDC windows in the hohlraum wall. The capsule composition and size are presented in top right box. As seen on the top view, the backlighter uses 22 beams to irradiate a Zn foil; a 5 μm slit is located between the backlighter and the capsule as a point projection source. The hohlraum aperture (0.55 mm width, 0.2 mm height) then defines the field of view and the detector is a streak camera.

growth. This hypothesis has motivated the elaboration of a new indirect drive implosion design, that uses the same mitigation strategy but this time at the fuel-ablator interface, called SQ-n [scaling (S) and quality (Q)] to achieve higher DT fuel compression [25,30]. The SQ-n design uses a ramp in the foot of the laser pulse (see Fig. 1, $t$ in the 2 to 4 ns range) to drive an accelerating first shock through the ablator to largely replace RM growth with stable RT oscillations, as shown in Fig. 2. A second shock is then launched to merge with the first shock just inside the DT ice-gas boundary, similar to the HDC design.

Specifically, the SQ-n is designed to create a $\sim$10–20 $\mu\mathrm{m\,ns^{-2}}$ acceleration of the DT fuel-ablator interface after the first shock as shown in its velocity (Fig. 1, dashed blue). Since the initial Atwood number at that interface, $A = (\rho_{\mathrm{ablator}} - \rho_{\mathrm{fuel}})/(\rho_{\mathrm{ablator}} + \rho_{\mathrm{fuel}})$, where $\rho_{\mathrm{ablator}}$ and $\rho_{\mathrm{fuel}}$ are the mass densities of the ablator and fuel, respectively, is negative (stable), this acceleration induces oscillation of the RM initiated perturbations due to the apparition of RT perturbations, with a maximum amplitude of $h_0\sqrt{1 + \Delta V^2 Ak/g}$, where $h_0$ is the initial perturbation height, $\Delta V$ is the jump in interface velocity, $g$ is the acceleration and $k$ is the wave number, rather than linear RM growth [26–29,31]. The growth due to this SQ-n acceleration, is shown in Fig. 2 showing that the benefit of the oscillation is starting to be significant for high mode number, about an order of magnitude after mode 2000. A significant reduction of growth rate during the RM phase will reduce the seeds for the RT phase, resulting in much less mixing during peak compression (stagnation) than for the HDC design.

In this Letter we measure for the first time the fuel-ablator interface acceleration as a function of the initial drive history. This is challenging and it requires a resolution of $\pm 5$ $\mu\mathrm{m\,ns^{-2}}$ (Fig. 1) for differentiating the HDC and SQ-n designs. Until recently, the existing experiments on the NIF did not have the capability to image the interface or achieve such resolution. Streaked refraction enhanced radiography (RER), a type of x-ray phase contrast imaging proposed earlier [32–35], was recently developed for NIF capsule implosions [35] and other experiments [36]. RER was demonstrated to image in-flight capsule density gradients such as the fuel-ablator interface that is not visible in traditional absorption only radiography [37]. To reach the required sensitivity, our RER arrangement was further improved by optimizing the backlighter geometry and material to increase the image signal-to-noise ratio (SNR) by $> 2\times$.

The results presented here will demonstrate that with RER we are able, for the first time, to measure the interface acceleration with required accuracy, confirming the effect of the drive change (Fig. 1) from HDC to SQ-n. RER will be used in the future to test the stability of new ICF designs.

RER of capsule implosions were conducted at the NIF for the HDC and SQ-n designs with a layout shown in Fig. 3. The typical DT layer was replaced with a tritium-hydrogen-deuterium (75% H, 24.2% T, 0.8% D) to reduce

the fusion neutron yield and associated background onto the RER imager, while retaining the same layer mass density as a DT implosion (50% D, 50% T). For the HDC implosion, we used an undoped HDC ablator capsules with 844 μm inner radius, 64 μm shell thickness and a 53 μm thick THD layer in depleted uranium (DU) hohlraum (10.13 mm length, 5.75 mm diam, 3.37 mm LEH size) filled with He gas at low density (0.3 mg cm$^{-3}$) [38]. For the SQ-n, the same capsule was used with a thinner 43 μm ice layer and a gold (Au) hohlraum (10.13 mm length, 5.40 mm diam, 3.45 mm LEH size), also filled with He at the same density. Removing the capsule dopant does not adversely affect the implosion dynamics at early times when little to no hohlraum radiation preheat [5] is generated and at the same time it improves the RER contrast to density gradients. In both experiments, 160 NIF beams drive the hohlraum with 0.783 and 1.015 MJ total energy, representing variants of the laser pulse shape of actual implosions that are truncated at late times to reduce hohlraum radiation preheat background onto the RER imager. A 5 μm wide imaging slit, backlit by four NIF quads (16 beams) heating a 12 μm thick Zn foil, generates the RER x-ray source with a ∼2 ns duration [39].

The Fig. 3 RER arrangement probes a capsule limb at its waist (facing the hohlraum midplane) during the implosion and tracks both the fuel-ablator interface trajectory as well as the shock evolution inside the ablator. Compared to [35,39], to further improve the contrast of the interfaces at early time ($t$ in the 2.5–4.5 ns range, see Fig. 1), we increased the magnification from 60× to 87× and the backlighter energy from 7.8 (Ni He$_\alpha$) to 9 keV (Zn He$_\alpha$). To avoid the blurring of fringes, the maximum allowable RER source size $S_c$ in μm [33] is

$$S_c = 3\left(p\Delta n[10^{-6}]\sqrt{\left(\frac{R}{2}\right)}\right)^{\frac{2}{3}}, \tag{1}$$

where $p$ is the distance between the source and the probed region and $R$ the capsule radius, both in cm. $\Delta n$ is the refractive index jump $= \Delta n_e/2n_c$ in $10^{-6}$ units, where $\Delta n_e$ for materials of $K$-shell ionization potential < photon energy is the total free and bound electron density jump, and $n_c$ is the probe photon energy critical density ($6 \times 10^{28}$ cm$^{-3}$ at 9 keV). Under our conditions, $S_c < 7$ μm. The expected interface velocity is $< 40$ μm ns$^{-1}$ during first shock for both designs (Fig. 1), hence for the 5.8 μm slit the integration time can be 100 ps to keep motion blur $< S_c$. This is 4× larger integration time than [35] that was probing the implosion at later time (higher implosion velocities) and hence improves the RER data quality through a 2× higher signal-to-noise ratio (SNR).

HYDRA postshot simulations [40] are used to generate synthetic streaked RER images using the equation available in Ref. [33] and the spatial and motional blurring of the experiment. As shown in the top images of Fig. 4, RER images can be decomposed in 3 regions: the inside of the capsule, the capsule ablator, and the region outside the capsule ablation front (that appears as a bright fringe in the images, exceeding the incident x-ray peak emission), consisting of He hohlraum gas fill and ablated material. Inside the ablator we see dark fringes traveling from outside of the capsule towards the ice ablator interface—these are the first, second (for traditional HDC design), and final shocks. Another visible dark fringe that starts when the first shock reaches the fuel-ablator interface and propagates backwards is the rarefaction wave reflecting from the interface. The two top figures of Fig. 4 that are the simulated RER images are compared to the two bottom figures of Fig. 4 that are the shot data for both the traditional HDC design (bottom left-hand side images) and for the SQ-n (bottom right-hand side images). This is the first time such measurement is possible in capsule implosion experiments, allowing the observation of interfaces (ablation front and fuel-ablator) trajectory as well as the shock propagation in the ablator. All the features and the trajectories measured in the data for both ablation front and ice-ablator interface show a very good correspondence with the simulations for both HDC and SQ-n implosions. They also show that, while for the HDC implosion 3 shocks are visible, for the SQ-n there are only two shocks and a rarefaction wave visible inside the shell region due to change in the laser drive as previously mentioned (Fig. 1).

The fuel-ablator interface trajectory tracing allowed the inference of its velocity plotted on Fig. 5. We observe a good agreement in interface velocity between the shot data and the simulations for both implosion designs. The trajectory was measured by finding the inflection point of the refraction fringes at each time. The precision of finding an inflection point on a sigmoid-shaped edge is considerably better than the system spatial resolution given by the source size $S_c = 5.8$ μm. It is given by $L/(2.35\mathrm{SNR}\sqrt{L/S_c}) = \pm 0.14$ μm, where $L$ is the scale length of the fringe = 8.5 μm, SNR is the signal to noise ratio per resolution element at the inflection point typically 21, and the 2.35 represents the normal distribution ratio of FWHM to standard deviation width. An 80 ps integration time between consecutive time steps was used, resulting in a velocity accuracy of $\pm 0.14/0.08 = \pm 1.8$ μm ns$^{-1}$. As we are looking for the acceleration difference 1 ns after the shock breakout, it means that the error on acceleration is $\pm 1.8$ μm ns$^{-2}$.

In the HDC design a constant velocity between the first and second shocks breakouts, hence no acceleration can be observed. By contrast, the SQ-n data shows an acceleration of the ice-ablator interface of $20 \pm 1.8$ μm ns$^2$, close to the simulated 18.3 μm ns$^{-2}$. This measured difference in the ice-ablator interface velocity confirms the intended SQ-n design change, aimed to stabilize the interface like the

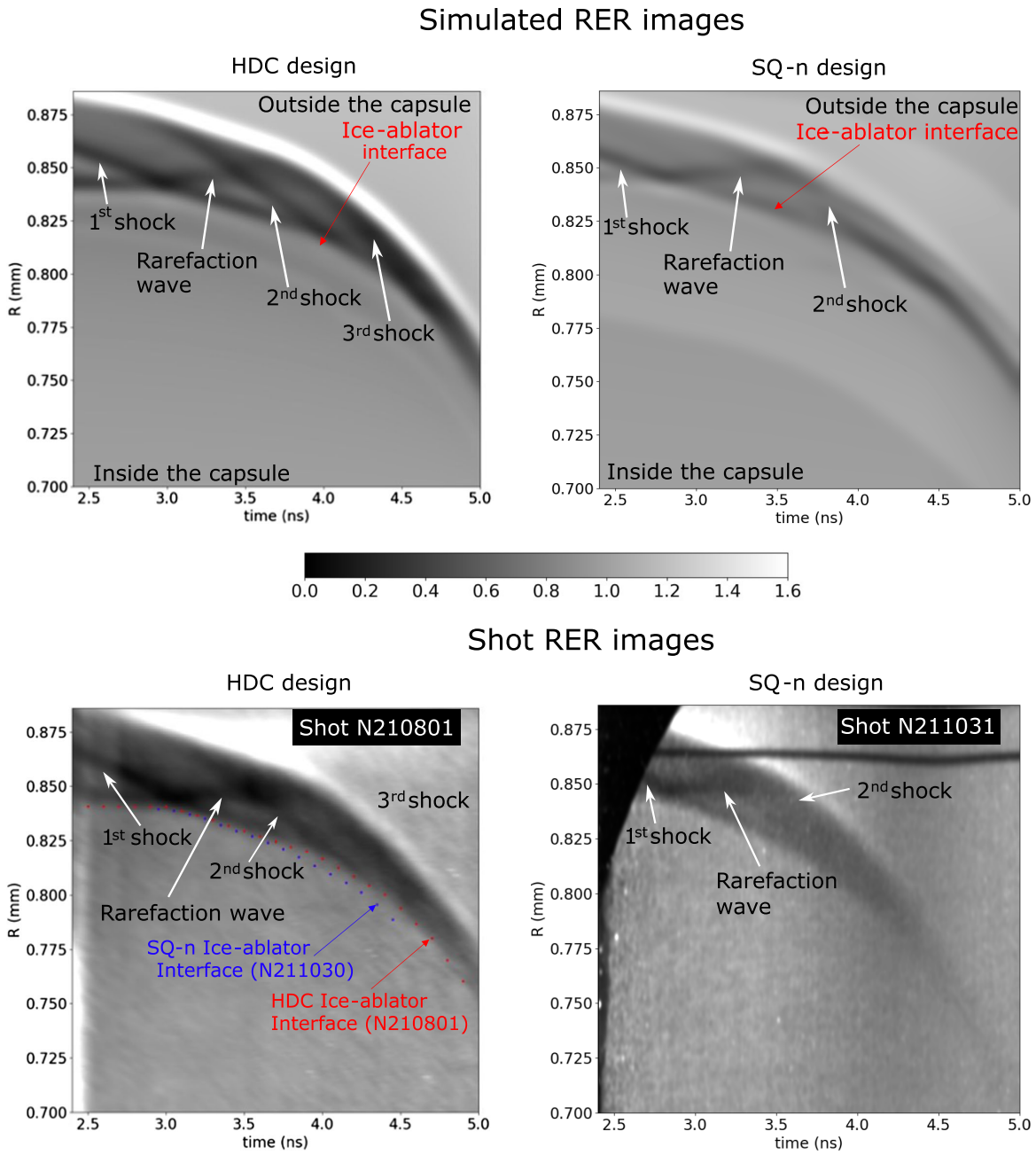


FIG. 4. Simulated RER streak image of the HDC design (top left) and of the SQ-n design (top right). The difference of the shock physics between the two designs is apparent: the HDC design has 3 shocks launched every 1 ns where the SQ-n design only two shocks; RER image of N210801 experiment for the HDC design (bottom left) shows 1st, 2nd, 3rd shocks as well as the rarefaction wave as simulated; RER image of N211030 experiment for the SQ-n implosion that shows 1st, 2nd shocks as well as the rarefaction wave as simulated. The blue dots show the fuel-ablator interface trajectory measured for SQ-n (N211030), and the red dots are for HDC (N210801) and are plotted on the same image to highlight their difference. All figures use the same color bar displayed in the middle.

BigFoot design [30] when compared to traditional HDC implosions.

In conclusion, the RER technique allowed, for the first time, the measurement of the fuel-ablator interface acceleration with high sensitivity ($\pm 1.8\ \mu\mathrm{m\,ns^{-2}}$) as well as the shock propagation inside the capsule ablator. These experimental results show that we can control and measure to high accuracy the interface acceleration after first shock passage and compare different implosion designs. In the case of the SQ-n design, a smooth acceleration of the fuel-ablator interface is a sign of improved early-time stability through the reduction of the instability's seeds. This improvement is expected to deliver a higher compression and to achieve higher neutron yield and will be tested in

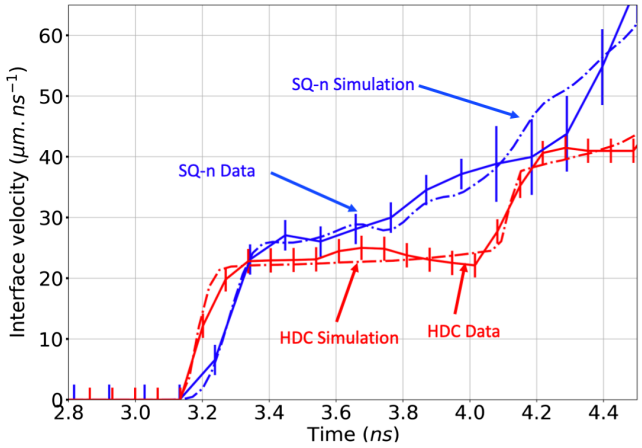


FIG. 5. (dash-dotted red line) Post-shot simulated fuel-ablator interface velocity of the HDC implosion and measured (solid red line), acceleration measurement error is $\pm 1.8\ \mu m\, ns^{-2}$; similar velocities for the SQ-n implosion simulated (dash-dotted blue line) and measured (solid blue line). The SQ-n data and simulations have been shifted 260 ps later to allow the comparison with the HDC results.

future experiments. The RER technique is a powerful tool to assess the performance of future designs that are looking to achieve multi-MJ yields through improved compression.

The authors would like to acknowledge NIF target fabrication, facility and operations for help in fielding these experiments. This work was performed under the auspices of the U.S. Department of Energy by Lawrence Livermore National Laboratory under Contract No. DE-AC52-07NA27344. The contributions of NIF operations and target fabrication teams to the success of these experiments are acknowledged. This document was prepared as an account of work sponsored by Lawrence Livermore National Laboratory, an agency of the U.S. government. Neither the U.S. government nor Lawrence Livermore National Security, LLC, nor any of their employees makes any warranty, expressed or implied, or assumes any legal liability or responsibility for the accuracy, completeness, or usefulness of any information, apparatus, product, or process disclosed, or represents that its use would not infringe privately owned rights. Reference herein to any specific commercial product, process, or service by trade name, trademark, manufacturer, or otherwise does not necessarily constitute or imply its endorsement, recommendation, or favoring by the U.S. government or Lawrence Livermore National Security, LLC. The views and opinions of authors expressed herein do not necessarily state or reflect those of the U.S. government or Lawrence Livermore National Security, LLC, and shall not be used for advertising or product endorsement purposes. LLNL-JRNL-836109.

*do6@llnl.gov

[1] G. H. Miller, E. I. Moses, and C. R. Wuest, The national ignition facility: Enabling fusion ignition for the 21st century, Nucl. Fusion **44**, S228 (2004).
[2] J. Lindl, Development of the indirect drive approach to inertial confinement fusion and the target physics basis for ignition and gain, Phys. Plasmas **2**, 3933 (1995).
[3] S. Atzeni and J. Meyer-ter Vehn, *The Physics of Inertial Fusion* (OUP, Oxford, 2004).
[4] E. I. Moses, J. Atherton, L. Lagin, D. Larson, C. Keane, B. MacGowan, R. Patterson, M. Spaeth, B. V. Wonterghem, P. Wegner, and R. Kauffman, The national ignition facility: Transition to a user facility, J. Phys. **688**, 012073 (2016).
[5] J. Lindl, O. Landen, J. Edwards, and E. Moses, Review of the national ignition campaign 2009–2012, Phys. Plasmas **21**, 020501 (2014).
[6] L. B. Hopkins *et al.*, Toward a burning plasma state using diamond ablator inertially confined fusion (ICF) implosions on the national ignition facility (NIF), Plasma Phys. Controlled Fusion **61**, 014023 (2019).
[7] A. L. Kritcher *et al.*, Design of inertial fusion implosions reaching the burning plasma regime, Nat. Phys. **18**, 251 (2022).
[8] A. B. Zylstra *et al.*, Burning plasma achieved in inertial fusion, Nature (London) **601**, 542 (2022).
[9] N. B. Meezan *et al.*, Cryogenic tritium-hydrogen-deuterium and deuterium-tritium layer implosions with high density carbon ablators in near-vacuum hohlraums, Phys. Plasmas **22**, 062703 (2015).
[10] D. S. Clark, C. R. Weber, J. L. Milovich, A. E. Pak, D. T. Casey, B. A. Hammel, D. D. Ho, O. S. Jones, J. M. Koning, A. L. Kritcher, M. M. Marinak, L. P. Masse, D. H. Munro, M. V. Patel, P. K. Patel, H. F. Robey, C. R. Schroeder, S. M. Sepke, and M. J. Edwards, Three-dimensional modeling and hydrodynamic scaling of national ignition facility implosions, Phys. Plasmas **26**, 050601 (2019).
[11] P. K. Patel *et al.*, Hotspot conditions achieved in inertial confinement fusion experiments on the national ignition facility, Phys. Plasmas **27**, 050901 (2020).
[12] L. Divol *et al.*, Symmetry control of an indirectly driven high-density-carbon implosion at high convergence and high velocity, Phys. Plasmas **24**, 056309 (2017).
[13] S. Le Pape *et al.*, Observation of a Reflected Shock in an Indirectly Driven Spherical Implosion at the National Ignition Facility, Phys. Rev. Lett. **112**, 225002 (2014).
[14] R. D. Richtmyer, Taylor instability in shock acceleration of compressible fluids, Commun. Pure Appl. Math. **13**, 297 (1960),
[15] E. E. Meshkov, Instability of the interface of two gases accelerated by a shock wave, Fluid Dyn. **4**, 101 (1969).
[16] G. Dimonte and B. Remington, Richtmyer-Meshkov Experiments on the Nova Laser at High Compression, Phys. Rev. Lett. **70**, 1806 (1993).
[17] L. Rayleigh, Investigation of the character of the equilibrium of an incompressible heavy fluid of variable density, Sci. Papers **II**, 200 (1900).
[18] G. I. Taylor, The formation of a blast wave by a very intense explosion I. Theoretical discussion, Proc. R. Soc. A **201**, 159 (1950).

[19] K. A. Flippo *et al.*, Late-time mixing and turbulent behavior in high-energy-density shear experiments at high Atwood numbers, Phys. Plasmas **25**, 056315 (2018).
[20] F. W. Doss, J. L. Kline, K. A. Flippo, T. S. Perry, B. G. DeVolder, I. Tregillis, E. N. Loomis, E. C. Merritt, T. J. Murphy, L. Welser-Sherrill, and J. R. Fincke, The shock/shear platform for planar radiation-hydrodynamics experiments on the national ignition facility, Phys. Plasmas **22**, 056303 (2015).
[21] S. E. Bodner, D. G. Colombant, J. H. Gardner, R. H. Lehmberg, S. P. Obenschain, L. Phillips, A. J. Schmitt, J. D. Sethian, R. L. McCrory, W. Seka, C. P. Verdon, J. P. Knauer, B. B. Afeyan, and H. T. Powell, Direct-drive laser fusion: Status and prospects, Phys. Plasmas **5**, 1901 (1998).
[22] V. N. Goncharov, J. P. Knauer, P. W. McKenty, P. B. Radha, T. C. Sangster, S. Skupsky, R. Betti, R. L. McCrory, and D. D. Meyerhofer, Improved performance of direct-drive inertial confinement fusion target designs with adiabat shaping using an intensity picket, Phys. Plasmas **10**, 1906 (2003).
[23] K. Anderson and R. Betti, Theory of laser-induced adiabat shaping in inertial fusion implosions: The decaying shock, Phys. Plasmas **10**, 4448 (2003).
[24] R. Betti, K. Anderson, J. Knauer, T. J. B. Collins, R. L. McCrory, P. W. McKenty, and S. Skupsky, Theory of laser-induced adiabat shaping in inertial fusion implosions: The relaxation method, Phys. Plasmas **12**, 042703 (2005).
[25] N. Metzler, A. L. Velikovich, and J. H. Gardner, Reduction of early-time perturbation growth in ablatively driven laser targets using tailored density profiles, Phys. Plasmas **6**, 3283 (1999).
[26] V. N. Goncharov, Theory of the Ablative Richtmyer-Meshkov Instability, Phys. Rev. Lett. **82**, 2091 (1999).
[27] Y. Aglitskiy, A. L. Velikovich, M. Karasik, V. Serlin, C. J. Pawley, A. J. Schmitt, S. P. Obenschain, A. N. Mostovych, J. H. Gardner, and N. Metzler, Direct Observation of Mass Oscillations due to Ablative Richtmyer-Meshkov Instability in Plastic Targets, Phys. Rev. Lett. **87**, 265001 (2001).
[28] O. V. Gotchev, V. N. Goncharov, J. P. Knauer, T. R. Boehly, T. J. B. Collins, R. Epstein, P. A. Jaanimagi, and D. D. Meyerhofer, Test of Thermal Transport Models Through Dynamic Overpressure Stabilization of Ablation-Front Perturbation Growth in Laser-Driven CH Foils, Phys. Rev. Lett. **96**, 115005 (2006).
[29] V. N. Goncharov, O. V. Gotchev, E. Vianello, T. R. Boehly, J. P. Knauer, P. W. McKenty, P. B. Radha, S. P. Regan, T. C. Sangster, S. Skupsky, V. A. Smalyuk, R. Betti, R. L. McCrory, D. D. Meyerhofer, and C. Cherfils-Clérouin, Early stage of implosion in inertial confinement fusion: Shock timing and perturbation evolution, Phys. Plasmas **13**, 012702 (2006).
[30] D. S. Clark, D. T. Casey, C. R. Weber, O. S. Jones, K. L. Baker, E. L. Dewald, L. Divol, A. Do, A. L. Kritcher, O. L. Landen, M. Millot, J. L. Milovich, V. A. Smalyuk, D. J. Strozzi, A. E. Pak, R. Tommasini, and M. J. Edwards, Exploring implosion designs for increased compression on the national ignition facility using high density carbon ablators, Phys. Plasmas **29**, 052710 (2022).
[31] C. R. Weber, D. S. Clark, D. T. Casey, O. Hall, G. N. andJones, O. Landen, A. E. Pak, and V. A. Smalyuk, Reduced Mixing in Inertial Confinement Fusion with Early-Time Interface Acceleration, Phys. Rev. E (2022).
[32] A. Pogany, D. Gao, and S. W. Wilkins, Contrast and resolution in imaging with a microfocus x-ray source, Rev. Sci. Instrum. **68**, 2774 (1997).
[33] J. A. Koch, O. L. Landen, B. J. Kozioziemski, N. Izumi, E. L. Dewald, J. D. Salmonson, and B. A. Hammel, Refraction-enhanced x-ray radiography for inertial confinement fusion and laser-produced plasma applications, J. Appl. Phys. **105**, 113112 (2009).
[34] J. A. Koch, O. L. Landen, L. J. Suter, L. P. Masse, D. S. Clark, J. S. Ross, A. J. Mackinnon, N. B. Meezan, C. A. Thomas, and Y. Ping, Refraction-enhanced backlit imaging of axially symmetric inertial confinement fusion plasmas, Appl. Opt. **52**, 3538 (2013).
[35] E. Dewald, O. Landen, D. Ho, L. Berzak Hopkins, Y. Ping, L. Masse, D. Thorn, J. Kroll, and A. Nikroo, Direct observation of density gradients in ICF capsule implosions via streaked refraction enhanced radiography (RER), High Energy Density Phys. **36**, 100795 (2020).
[36] A. Kar, T. R. Boehly, P. B. Radha, D. H. Edgell, S. X. Hu, P. M. Nilson, A. Shvydky, W. Theobald, D. Cao, K. S. Anderson, V. N. Goncharov, and S. P. Regan, Simulated refraction-enhanced x-ray radiography of laser-driven shocks, Phys. Plasmas **26**, 032705 (2019).
[37] E. L. Dewald *et al.*, Capsule ablator inflight performance measurements via streaked radiography of ICF implosions on the NIF, J. Phys. **688**, 012014 (2016).
[38] R. E. Olson, R. J. Leeper, S. A. Yi, J. L. Kline, A. B. Zylstra, R. R. Peterson, R. Shah, T. Braun, J. Biener, B. J. Kozioziemski, J. D. Sater, M. M. Biener, A. V. Hamza, A. Nikroo, L. B. Hopkins, D. Ho, S. LePape, and N. B. Meezan, Wetted foam liquid fuel ICF target experiments, J. Phys. **717**, 012042 (2016).
[39] E. L. Dewald, O. L. Landen, L. Masse, D. Ho, Y. Ping, D. Thorn, N. Izumi, L. Berzak Hopkins, J. Kroll, A. Nikroo, and J. A. Koch, X-ray streaked refraction enhanced radiography for inferring inflight density gradients in ICF capsule implosions, Rev. Sci. Instrum. **89**, 10G108 (2018).
[40] M. M. Marinak, G. D. Kerbel, N. A. Gentile, O. Jones, D. Munro, S. Pollaine, T. R. Dittrich, and S. W. Haan, Three-dimensional hydra simulations of national ignition facility targets, Phys. Plasmas **8**, 2275 (2001).